THE EUROPEAN
PHYSICAL JOURNAL C

Analysis of the $\psi(4040)$ and $\psi(4160)$ decay into $D^{(*)}\bar{D}^{(*)}$, $D_s^{(*)}\bar{D}_s^{(*)}$

M. Bayar[1,2,a], **N. Ikeno**[2,3,b], **E. Oset**[2,4,c]

[1] Department of Physics, Kocaeli University, Izmit 41380, Turkey
[2] Departamento de Física Teórica and IFIC, Centro Mixto Universidad de Valencia-CSIC Institutos de Investigación de Paterna, Aptdo.22085, 46071 Valencia, Spain
[3] Department of Agricultural, Life and Environmental Sciences, Tottori University, Tottori 680-8551, Japan
[4] Department of Physics, Guangxi Normal University, Guilin 541004, China

Abstract We have performed an analysis of the $e^+e^- \to D^{(*)}\bar{D}^{(*)}$ data in the region of the $\psi(4040)$ and $\psi(4160)$ resonances which have a substantial overlap and require special care. By using the $^3P_0$ model to relate the different $D^{(*)}\bar{D}^{(*)}$ production modes, we make predictions for production of these channels and compare with experiment and other theoretical approaches. As a side effect we find that these resonances qualify largely as $c\bar{c}$ states and the weight of the meson–meson components in the wave function is very small.

1 Introduction

The charmonium spectroscopy has been studied both theoretically and experimentally over four decades, but there are still many debates in charmonium physics. Although the charmonium system is well described below the open charm threshold, for the charmonium states above the open charm threshold there is no real consensus between experimental information and theoretical results. Above the open charm threshold charmonium states can decay into several two body final states as stated in Refs. [1,2], the decay channels are $\psi(4040) \to D\bar{D}, D\bar{D}^*, D^*\bar{D}, D^*\bar{D}^*, D_s\bar{D}_s, \psi(4160) \to D\bar{D}, D\bar{D}^*, D^*\bar{D}, D^*\bar{D}^*, D_s\bar{D}_s, D_s\bar{D}_s^*, D_s^*\bar{D}_s$. It is also important to consider charm meson production to understand the hadron spectrum well.

Experimental research has been done to determine masses and total widths of the $\psi(4040)$ and $\psi(4160)$ states. For instance, the total cross section for hadron production in e^+e^- annihilation was analysed in Ref. [3]. They measured R values, which is defined as $R = \sigma(e^+e^- \to hadrons)/$

$\sigma(e^+e^- \to \mu^+\mu^-)$ with the BESII detector at center-of-mass energies between 3.7 and 5.0 GeV. They show the R values for the high mass charmonia structure in Fig. 1 of Ref. [3] where the two resonances have some overlap. In the analysis they use an energy dependent total width and introduce relative phases between the resonances in the fit. They conclude that the results are sensitive to the form of the energy-dependent total width, and the influence of the phase angles of the resonance parameters is important. The e^+e^- annihilation with exclusive production of $D\bar{D}, D\bar{D}^*, D^*\bar{D}^*$ was investigated in Ref. [4]. The authors mention that interference between the resonances and noresonance contributions is required to obtain a satisfactory description of the data, somewhat a different interpretation than that of Ref. [3]. They also measured $\Gamma(\psi(4040) \to D\bar{D})/\Gamma(\psi(4040) \to D^*\bar{D})$ and find $0.24 \pm 0.05 \pm 0.12$ and compare with a calculation using the $^3P_0$ model of Ref. [2]. The agreement is not good. It is not clear how the spin-angular momentum algebra is done for the $^3P_0$ model in Ref. [2].

The quantum numbers assigned to the $\psi(4040)$ and $\psi(4160)$ are 3^3S_1 and 2^3D_1 in Ref. [2], respectively. The same assignment is done in Refs. [5–7]. The decay widths of the $\psi(4040)$ and $\psi(4160)$ had been evaluated in the $^3P_0$ model (Table X and XII in Ref. [2]) and also in Ref. [4] (Table VI). The results are very different. In Ref. [8], the authors calculate $\Gamma(\psi(4040) \to D^0\bar{D}^0)/\Gamma(\psi(4040) \to D^{0*}\bar{D}^0 + cc) = 0.05 \pm 0.03$. Yet, this seems to be in contradiction with the results of Ref. [4].

As one can see, there is no noconsensus on the interpretation of the data. Inclusive and exclusive cross sections for D^+, D^-, and D_s^* production in e^+e^- annihilation are also available from Ref. [9]. There are further data from Belle [10], where measurements of $e^+e^- \to D^{(*)\pm}D^{*\mp}$ using initial state radiation are done. Further data from BES on $e^+e^- \to hadrons$ are available in [11,12], which are analyzed in [13] in terms of three resonances, $\psi(4040), \psi(4160), \psi(4415)$,

a e-mail: melahat.bayar@kocaeli.edu.tr (corresponding author)
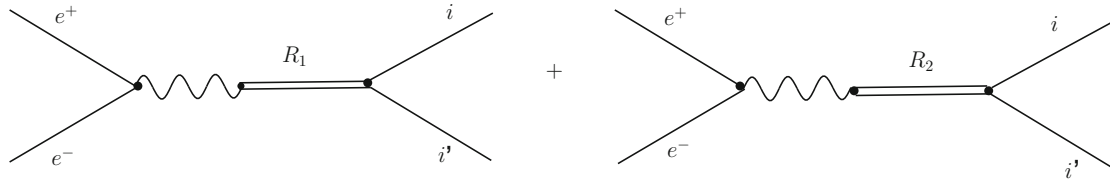
b e-mail: ikeno@tottori-u.ac.jp

c e-mail: oset@ific.uv.es

Fig. 1 Feynman diagrams of $e^+e^- \to R_1(R_2) \to i\,i'$, where $R_1 \equiv \psi(4040)$ and $R_2 \equiv \psi(4160)$ and i, i' correspond to any of the $D^0\bar{D}^0, D^+\bar{D}^-$, $D^0\bar{D}^{*0}, D^{*0}\bar{D}^0, D^{*+}\bar{D}^-, D^+\bar{D}^{*-}, D^{*0}\bar{D}^{*0}, D^{*+}\bar{D}^{*-}, D_s^+\bar{D}_s^-, D_s^+\bar{D}_s^{*-}, D_s^{*+}\bar{D}_s^-, D_s^{*+}\bar{D}_s^{*-}$ channels
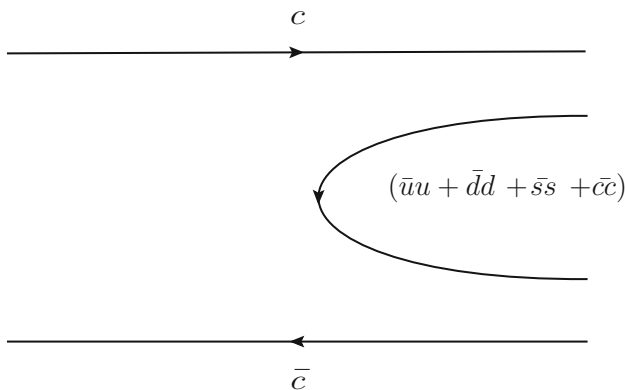

Fig. 2 Hadronization process for $\psi(4040)[\psi(4160)] \to ii'$

with interference among them. We shall not consider the $\psi(4415)$, which is far away and disconnected from the other two resonances and concentrate on the $\psi(4040)$ and $\psi(4160)$ which overlap in the hadron production spectrum.

This paper is organized as follows. In Sect. 2, we establish the formalism of calculating the cross section for $e^+e^- \to$ hadrons through the dressed propagator of the $\psi(4040)$ and $\psi(4160)$, In Sect. 3, we present the results on the line shape of the $\psi(4040)$ and $\psi(4160)$ fitting to the experimental data, the meson–meson probabilities in the $\psi(4040)$ and $\psi(4160)$ wave functions and the Z probabilities using the parameters extracted from the fitting. A summary and conclusion is presented in Sect. 4.

2 Formalism

The Feynman diagrams of hadron production in e^+e^- annihilation for $\psi(4040)$ and $\psi(4160)$ are shown in Fig. 1. The first part of the Feynman diagrams in Fig. 1 is the electromagnetic interaction and the second part of the diagrams is strong interaction. In the second part, we assume the ψ resonances to be $c\bar{c}$ states and insert a $\bar{q}q$ pair with the quantum numbers of the vacuum between the $c\bar{c}$, the quark components of the $\psi(4040)$ and $\psi(4160)$, in order to produce the

$D^{(*)}\bar{D}^{(*)}$ pairs. This is called hadronization and the mechanism of hadronization is shown in Fig. 2.

We show the hadronization procedure in detail. We will include a $\bar{q}q$ pair with the quantum numbers of the vacuum and will obtain a pair of mesons. These meson pairs could be vector-vector (VV), pseudoscalar-vector (PV), vector-pseudoscalar (VP) or pseudoscalar-pseudoscalar (PP) meson. To do this, we first write the $\bar{q}q$ matrix M

$$M = (q\bar{q}) = \begin{pmatrix} u\bar{u} & u\bar{d} & u\bar{s} & u\bar{c} \\ d\bar{u} & d\bar{d} & d\bar{s} & d\bar{c} \\ s\bar{u} & s\bar{d} & s\bar{s} & s\bar{c} \\ c\bar{u} & c\bar{d} & c\bar{s} & c\bar{c} \end{pmatrix}. \tag{1}$$

The hadronization in the flavor space proceeds as

$$c\bar{c} \to c \sum_{i=1}^{4} \bar{q}_i q_i \, \bar{c} = \sum_{i=1}^{4} c\bar{q}_i q_i \bar{c} = (MM)_{44}. \tag{2}$$

On the hadron level we can write the M matrix in terms of the physical mesons. This matrix M could be the vector or the pseudoscalar matrix. The vector matrix V is given by

$$V = \begin{pmatrix} \frac{1}{\sqrt{2}}\rho^0 + \frac{1}{\sqrt{2}}\omega & \rho^+ & K^{*+} & \bar{D}^{*0} \\ \rho^- & -\frac{1}{\sqrt{2}}\rho^0 + \frac{1}{\sqrt{2}}\omega & K^{*0} & \bar{D}^{*-} \\ K^{*-} & \bar{K}^{*0} & \phi & D_s^{*-} \\ D^{*0} & D^{*+} & D_s^{*+} & J/\psi \end{pmatrix}. \tag{3}$$

and the pseudoscalar matrix can be written as

$$P = \begin{pmatrix} \frac{1}{\sqrt{2}}\pi^0 + \frac{1}{\sqrt{3}}\eta + \frac{1}{\sqrt{6}}\eta' & \pi^+ & K^+ & \bar{D}^0 \\ \pi^- & -\frac{1}{\sqrt{2}}\pi^0 + \frac{1}{\sqrt{3}}\eta + \frac{1}{\sqrt{6}}\eta' & K^0 & D^- \\ K^- & \bar{K}^0 & -\frac{1}{\sqrt{3}}\eta + \sqrt{\frac{2}{3}}\eta' & D_s^- \\ D^0 & D^+ & D_s^+ & \eta_c \end{pmatrix}. \tag{4}$$

where the standard $\eta - \eta'$ mixing of Ref. [14] is used. Finally as we mentioned before, the hadronization gives rise to PP, PV, VP, VV in terms of two mesons and hence we have

$$(PP)_{4,4} = D^0\bar{D}^0 + D^+D^- + D_s^+D_s^-, \tag{5}$$

$$(PV)_{4,4} = D^0\bar{D}^{*0} + D^+D^{*-} + D_s^+D_s^{*-}, \tag{6}$$

$$(VP)_{4,4} = D^{*0}\bar{D}^0 + D^{*+}D^- + D_s^{*+}D_s^-, \tag{7}$$

$$(VV)_{4,4} = D^{*0}\bar{D}^{*0} + D^{*+}D^{*-} + D_s^{*+}D_s^{*-}. \tag{8}$$

where we have neglected η_c^2, $\eta_c \, J/\psi$, $J/\psi \, J/\psi$, since they are too heavy relative to the other channels.

Let us come back again to Fig. 1. First there is an interaction $e^+e^- \to R_{1(2)}$ and then decay of $R_{1(2)} \to i \, i'$ where $i \, i'$ correspond to the $D^0\bar{D}^0$, $D^+\bar{D}^-$, $D^0\bar{D}^{*0}$, $D^{*0}\bar{D}^{0}$, $D^{*+}\bar{D}^-$, $D^+\bar{D}^{*-}$, $D^{*0}\bar{D}^{*0}$, $D^{*+}\bar{D}^{*-}$, $D_s^+\bar{D}_s^-$, $D_s^+\bar{D}_s^{*-}$, $D_s^{*+}\bar{D}_s^-$, $D_s^{*+}\bar{D}_s^{*-}$ channels. The couplings of $e^+e^- \to R_1$ and $e^+e^- \to R_2$ are different and the couplings of $R_1 \to i \, i'$ and $R_2 \to i \, i'$ are also different. However, for each resonance we can relate the amplitude for $D^0\bar{D}^0$, $D^+\bar{D}^-$, $D^0\bar{D}^{*0}$, $D^{*0}\bar{D}^0$, $D^{*+}\bar{D}^-$, $D^+\bar{D}^{*-}$, $D^{*0}\bar{D}^{*0}$, $D^{*+}\bar{D}^{*-}$, $D_s^+\bar{D}_s^-$, $D_s^+\bar{D}_s^{*-}$, $D_s^{*+}\bar{D}_s^-$, $D_s^{*+}\bar{D}_s^{*-}$ production by means of the $^3P_0$ model used in the paper of Ref. [15]. In this model one uses the most basic $\bar{q}q$ configuration that provides the $\bar{q}q$ state with vacuum quantum numbers. Since $\bar{q}$ has negative parity we need $L = 1$ to restore the parity, which implies that the spin S is $S = 1$ such that the total angular momentum J can be $J = 0$. The spin angular momentum components are considered together with the spin of the $c\bar{c}$ components to finally provide the spin of the $D^{(*)}\bar{D}^{(*)}$ pairs, which are produced in p-wave. Details on the angular momentum algebra for the process are given in Ref. [15].

Now let us write the matrix element of the first part (electron-positron pair annihilation) of the Feynman diagrams of Fig. 1 as

$$t' \sim e\bar{v}(p_1)\gamma^\mu u(p_2)\epsilon_\mu(\gamma) \tag{9}$$

where $u(p_2)$ and $\bar{v}(p_1)$ are the spinors of the electron and positron, respectively and $\epsilon_\mu(\gamma)$ is the polarization of the photon. Then the square of the absolute value of the matrix element is obtained as follows

$$|t'|^2 \sim \frac{4e^2}{2m2m}(p_1^\mu p_2^\nu - p_1 \cdot p_2 g^{\mu\nu} + p_1^\nu p_2^\mu)\epsilon_\mu \epsilon_\nu \tag{10}$$

where the original photon polarizations $\epsilon_\mu \epsilon_\nu$ become the R polarization after $\gamma \to \psi$ conversion, and in the R rest frame only the spatial components of ϵ_μ remain. Then we write the whole matrix element as

$$t \sim e\bar{v}(p_1)\gamma^\mu u(p_2)\epsilon_\mu f_R \, D_R \, A_{Ri} \, p' \frac{1}{p_\gamma^2} \tag{11}$$

where D_R is a propagator of the R meson, f_R is a $\gamma \to \psi$ conversion factor and A_{Ri} the coupling of the R to each $i \, i'$ channels ($D^0\bar{D}^0$, $D^+\bar{D}^-$, $D^0\bar{D}^{*0}$, $D^{*0}\bar{D}^0$, $D^{*+}\bar{D}^-$, $D^+\bar{D}^{*-}$, $D^{*0}\bar{D}^{*0}$, $D^{*+}\bar{D}^{*-}$, $D_s^+\bar{D}_s^-$, $D_s^+\bar{D}_s^{*-}$, $D_s^{*+}\bar{D}_s^-$, $D_s^{*+}\bar{D}_s^{*-}$). We can take the spatial component of ϵ_μ contracted in $|t|^2$ as $\sum \epsilon_i \epsilon_j \to \delta_{ij}$ with $i, j = 1, 2, 3$, so we have

$$|t|^2 \sim \frac{e^2}{2m2m}M_{\text{inv}}^2|f_R \, D_R \, A_{Ri} \, p'|^2\left(\frac{1}{p_\gamma^2}\right)^2. \tag{12}$$
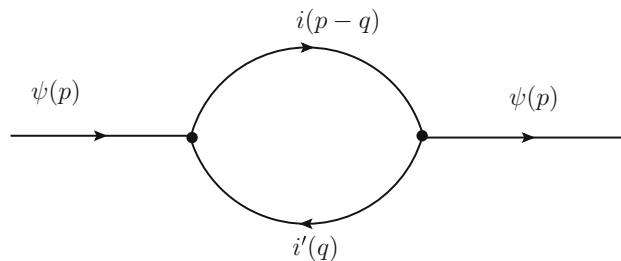

Fig. 3 The ψ propagator dressed with a $i \, i'$ loop

Once we get $|t|^2$, we can calculate the cross section as follows

$$\sigma = 4\pi\frac{d\sigma}{d\Omega} \sim \frac{1}{16\,\pi}\frac{1}{s}e^2 M_{\text{inv}}^2\left(\frac{1}{p_\gamma^2}\right)^2\frac{p'}{p}|f_R \, D_R \, A_{Ri} \, p'|^2. \tag{13}$$

Using $M_{\text{inv}} = \sqrt{s}$, then the cross section read as

$$\sigma = \frac{1}{8\,\pi}\frac{1}{s^2}\frac{1}{\sqrt{s}}e^2(p')^3|f_R \, D_R \, A_{Ri}|^2, \tag{14}$$

where p' is the meson momentum in the $M_i M_i'$ rest frame

$$p' = \frac{\lambda^{1/2}(s, M_i^2, M_i'^2)}{2\sqrt{s}}, \tag{15}$$

with M_i and M_i' the masses of the i, i' mesons and D_R the propagator of the R vector,

$$D_R = \frac{1}{p^2 - M_R^2 + iM_R\Gamma_R}, \tag{16}$$

with $p = p_1 + p_2$, in the case of a free vector.

Next, we include the meson–meson self energy in the vector propagator

$$D_R = \frac{1}{p^2 - M_R^2 - \Pi(p)}. \tag{17}$$

The ψ selfenergy diagrams are depicted in Fig. 3. In order to evaluate $\Pi(p^2)$ we indicate the dressing of ψ by meson–meson components and we include PP, VP, PV, and VV. There is only one unknown global parameter A_{Ri} since all the different $D^{(*)}\bar{D}^{(*)}$, $D_s^{(*)}\bar{D}_s^*$ channels can be connected via Eqs. (5–8) and the $^3P_0$ model, for which the details are given in [15]. In that work a detailed derivation was done for the case where the $c\bar{c}$ quarks in the ψ state are in D-wave, which is case for the $\psi(4160)$ according to Ref. [5] (2^3D_1). For S-wave, where the $\psi(4040)$ is classified according to Ref. [5] (3^3S_1), the calculations are done in a similar way and we provide here the new coefficients in analogy to those obtained for D-wave in [15], where the $\psi(3770)$ (1^3D_1 according to Ref. [5]) was studied.

The self energy contributions $\Pi(p)$ are shown in Fig. 3, and detailing the channels in Fig. 4, and is written as follows
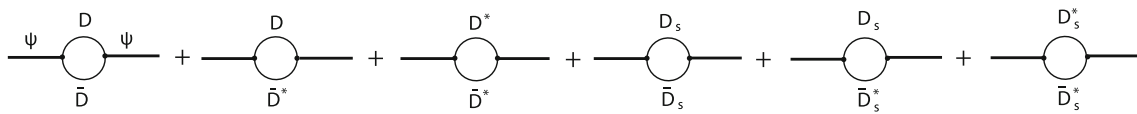
Fig. 4 Contribution to the ψ selfenergy for the vector ψ propagator dressed with a meson–meson loop with cc

$$-i\Pi_i(p) = \int \frac{d^4q}{(2\pi)^4}(-i)V_1(-i)V_2\frac{i}{q^2 - m_{D_i}^2 + i\varepsilon}$$
$$\times \frac{i}{(p-q)^2 - m_{D_{i'}}^2 + i\varepsilon}F(\boldsymbol{q})^2, \tag{18}$$

where p is the total four momentum of the system, and m_{D_i} and $m_{D_{i'}}$ are the masses of the mesons in the i, i'-channel. $F(\boldsymbol{q})$ is a form factor and the subindex of the D mesons indicates all twelve channels which means $i, i' = 1, 2, \ldots, 12$. We use the couplings of $\psi(4040)$ or $\psi(4160) \to PP, PV, VP, VV$ which have the effective form evaluated in the $^3P_0$ model, such that the sum over polarizations on the vector states in Π, Fig. 3, and in the final states, Fig. 1, are already done,

$$V_{\psi,(D_iD_{i'})} = A_{Ri}|\boldsymbol{q}| = A\,g_{R,i}|\boldsymbol{q}|, \tag{19}$$

where we separate the coupling A_{Ri} of $R \to$ meson–meson channel into a global constant A and the coefficient $g_{R,i}$ which stems from the $^3P_0$ model calculation. Then $\Pi(p)$ is rewritten as

$$\Pi_i(p) = i\,g_{R,i}^2 A^2 \int \frac{d^4q}{(2\pi)^4}\boldsymbol{q}^2 \frac{1}{q^2 - m_{D_i}^2 + i\varepsilon}$$
$$\times \frac{1}{(p-q)^2 - m_{D_{i'}}^2 + i\varepsilon}F(\boldsymbol{q})^2. \tag{20}$$

The q^0 integration can be evaluated analytically and then we get in the rest frame of the $\psi(4040)$ and $\psi(4160)$ ($p^0 = \sqrt{s}$)

$$\Pi(p^0) = A^2 \sum g_{R,i}^2 \, \tilde{G}_i(p^0), \tag{21}$$

where A is a global constant to be determined from the data, and $\tilde{G}_i(p^0)$ is

$$\tilde{G}_i(p^0) = \int \frac{dq}{(2\pi)^2}\frac{\omega_1(\boldsymbol{q}) + \omega_2(\boldsymbol{q})}{\omega_1(\boldsymbol{q})\omega_2(\boldsymbol{q})}$$
$$\times \frac{\boldsymbol{q}^4}{(p^0)^2 - (\omega_1(\boldsymbol{q}) + \omega_2(\boldsymbol{q}))^2 + i\varepsilon}F(\boldsymbol{q})^2, \tag{22}$$

where $\omega_1(\boldsymbol{q}) = \sqrt{\boldsymbol{q}^2 + m_{D_i}^2}$, $\omega_2(\boldsymbol{q}) = \sqrt{\boldsymbol{q}^2 + m_{D_{i'}}^2}$. Then the $g_{R,i}^2$ values in Eq. (21) are calculated for the $\psi(4040)$

Table 1 $g_{R,i}^2$ values for $\psi(4040)$ and $\psi(4160)$ vector mesons

Channels	$g_{R,i}^2$ for $\psi(4040)$	$g_{R,i}^2$ for $\psi(4160)$
$D^0\bar{D}^0$	1/12	1/12
$D^+\bar{D}^-$	1/12	1/12
$D^0\bar{D}^{*0}$	1/6	1/24
$D^{*0}\bar{D}^0$	1/6	1/24
$D^+\bar{D}^{*-}$	1/6	1/24
$D^{*+}\bar{D}^-$	1/6	1/24
$D^{*0}\bar{D}^{*0}$	7/12	77/120
$D^{*+}\bar{D}^{*-}$	7/12	77/120
$D_s^+\bar{D}_s^-$	1/12	1/12
$D_s^+\bar{D}_s^{*-}$	1/6	1/24
$D_s^{*+}\bar{D}_s^-$	1/6	1/24
$D_s^{*+}\bar{D}_s^{*-}$	7/12	77/120

($\psi(4160)$) like in Ref. [15] and the values are presented in Table 1.

As in Ref. [15], we take the form factor as follows

$$F(\boldsymbol{q})^2 = \frac{1 + (R\,q_{\rm on})^2}{1 + (R\,q)^2}, \quad q \equiv |\boldsymbol{q}|,$$
$$q_{\rm on} = \frac{\lambda^{1/2}(s, m_{D_i}^2, m_{D_{i'}}^2)}{2\sqrt{s}} \tag{23}$$

where R is a parameter. This factor is motivated by the Blatt–Weisskopf barrier penetration factor [16] which is often used in the parametrization of the width of resonances. If the channel is closed, we take $q_{\rm on} = 0$. Since $\tilde{G}_i(p^0)$ in Eq. (22) is logarithmically divergent, we have to make a subtraction and we do it such that the propagator has the pole at M_R. Hence the D_R propagator rewritten as

$$D_R(p) = \frac{1}{p^2 - M_R^2 - \Pi'(p)} \tag{24}$$

with $\Pi'(p) = \Pi(p) - \text{Re}\,\Pi(M_R)$.

Next step we have to take into account the two resonances. We use σ of Eq. (14) to obtain the cross section for production of the channel $i\,i'$, any of the $D^0\bar{D}^0, D^+\bar{D}^-, D^0\bar{D}^{*0}, D^{*0}\bar{D}^0, D^{*+}\bar{D}^-, D^+\bar{D}^{*-}, D^{*0}\bar{D}^{*0}, D^{*+}\bar{D}^{*-}, D_s^+\bar{D}_s^-, D_s^+\bar{D}_s^{*-}, D_s^{*+}\bar{D}_s^-, D_s^{*+}\bar{D}_s^{*-}$ channels. Then we must sum coherently the contribution of the two resonances $\psi(4040)$ and $\psi(4160)$. Hence, $f_R\,D_R\,A_{Ri}$ of Eq. (14) gets substituted by

Table 2 Three sets of fit data for nine parameters

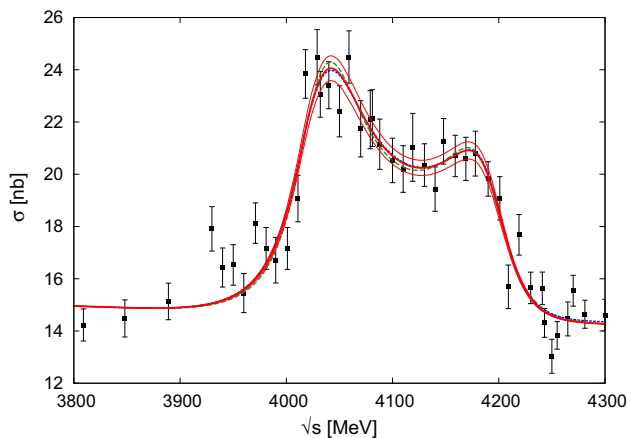| Parameters	Set I	Set II	Set III
M_{R_1} [MeV]	4036.34 ± 3.04	4035.95 ± 2.97	4036.73 ± 3.21
f_{R_1}	37.38 ± 1.37	35.75 ± 1.97	36.92 ± 1.49
A_1^2	149.99 ± 5.71	139.9 ± 3.15	153.9 ± 6.48
$R_1 [\text{MeV}^{-1}]$	$(8.71 \pm 4.36) \times 10^{-3}$	$(1.19 \pm 0.59) \times 10^{-2}$	$(7.41 \pm 3.71) \times 10^{-3}$
M_{R_2} [MeV]	4197.5 ± 7.95	4195.63 ± 4.56	4199.17 ± 11.21
f_{R_2}	30.92 ± 3.31	27.94 ± 11.76	25.47 ± 8.19
A_2^2	53.91 ± 7.35	56.12 ± 7.85	53.91 ± 14.56
$R_2 [\text{MeV}^{-1}]$	$(2.68 \pm 1.34) \times 10^{-3}$	$(2.23 \pm 1.12) \times 10^{-3}$	$(1.71 \pm 0.86) \times 10^{-3}$
ϕ [radian]	3.408 ± 0.283	3.207 ± 0.683	3.133 ± 0.474

Fig. 5 Total hadronic cross section of $\sigma(e^+e^- \rightarrow hadrons)$ fitted to the experimental data from Fig. 1 in Ref. [13]. The solid red line corresponds the parameters Set I, dashed green line Set II and dotted blue line Set III. The most extreme thin lines provide the band of uncertainty of the fit evaluated as explained in the tex
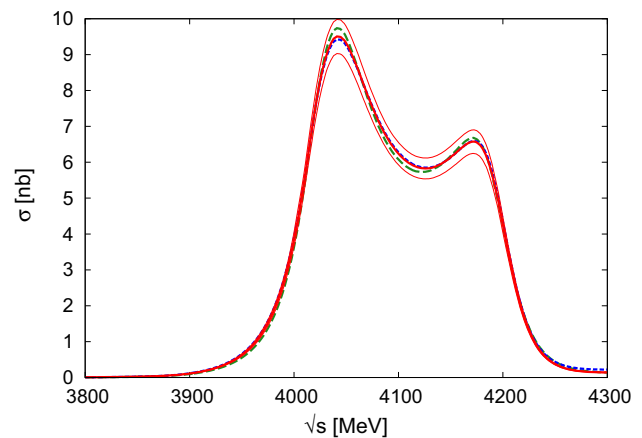

Fig. 6 The total hadronic cross section of $\sigma(e^+e^- \rightarrow hadrons)$ without background. The solid red line corresponds the parameters Set I, dashed green line Set II and dotted blue line Set III. The most extreme thin lines provide the band of uncertainty of the fit evaluated as explained in the tex

$f_{R1} D_{R1} A_{R1} g_{1i} + f_{R2} e^{i\phi} D_{R2} A_{R2} g_{2i}$, which includes a relative phase factor between the two terms. Then, the cross section is given by

$$\sigma_i = \frac{1}{8\pi} \frac{1}{s^2} \frac{1}{\sqrt{s}} e^2 (p')^3 |f_{R1} D_{R1} A_1 g_{1i}$$
$$+ f_{R2} e^{i\phi} D_{R2} A_2 g_{2i}|^2, \tag{25}$$

and vanishes for the channels which are closed at a given energy.

3 Results

The cross sections with the two resonances are obtained by means of Eq. (25). As we mention in the Sect. 2, both the couplings $e^+e^- \rightarrow R_{1(2)}$ and $R_{1(2)} \rightarrow i\,i'$ are different for particle 1 and 2, and then we have four parameters. The masses M_{R_1} and M_{R_2}, enter into $D_{R_1}(p)$ and $D_{R_2}(p)$ in Eq. (24), are also changed a bit with respect to the nominal

ones, such as to obtain the peak position as in the experiment. We will allow a relative phase between the two contributions, which means we will make the $e^+e^- \rightarrow R_2$ coupling complex. Hence f_{R_2} will be complex to take into account the mixing of the two resonances as the experimental papers all do, that is $f_{R_2} \rightarrow f_{R_2} e^{i\phi}$, thus we have the extra f_{R_1}, f_{R_2} and ϕ ($\phi \in [0, 2\pi]$) parameters. We have also A_1 and A_2 real positive parameters. We shall also use the parameter R in the form factor to control the convergence of the selfenergy integrals. So we have the R_1 and R_2 parameters for each resonance in Eq. (23). This means we have nine parameters in total.

We determine the nine parameters by performing a fit to the total hadronic cross section obtained as $\sigma(e^+e^- \rightarrow hadrons)$ [13]. We get the experimental data from Fig. 1 of [13] and include the same background as in Eq. (3) of Ref. [13] with the same parameterization. We obtained three sets of values for the free parameters which are written in Table 2, corresponding to different local minima of the χ^2 in the mul-
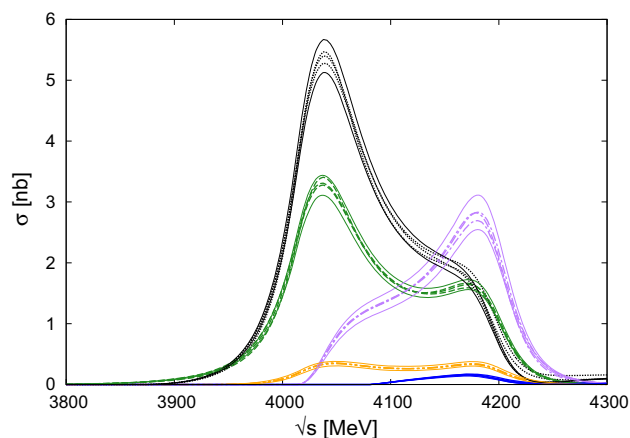
Fig. 7 Different hadronic cross section of $\sigma(e^+e^- \rightarrow i\,i')$ without background. The dashed green lines correspond to the $\sigma(D\bar{D})$, the black dotted lines the $\sigma(D\bar{D}^*)$, the purple dash-dotted lines the $\sigma(D^*\bar{D}^*)$, the orange two dot-dashed lines the $\sigma(D_s^+\bar{D}_s^-)$ and the blue solid lines the $\sigma(D_s\bar{D}_s^*)$ for Set I, Set II and Set III. The most extreme thin lines provide the band of uncertainty of the fit evaluated as explained in the tex

tidimensional space. We also show there the errors in the parameters obtained in the fit. The total hadronic cross section including background for three different sets of parameter are shown in Fig. 5. As we see from the figure, the results of the total cross section of $\sigma(e^+e^- \rightarrow hadrons)$ are similar with the three sets of parameters and they provide a good fit to the data, both above and below the peaks. In the figure, we also show the band of uncertainty in the fit, which is obtained making runs with random values for all the parameters within their uncertainty range, and then calculating the average and the dispersion. We also show the total hadronic cross section without background in Fig. 6, including the uncertainty band.

We also show the different contributions of the hadronic cross section in Fig. 7. The $\sigma(D\bar{D})$ includes two contributions, as the sum of $D^0\bar{D}^0 + D^+\bar{D}^-$, the $\sigma(D\bar{D}^*)$ four contributions, as the sum of $D^0\bar{D}^{*0} + D^{*0}\bar{D}^0 + D^{*+}\bar{D}^- + D^+\bar{D}^{*-}$, the $\sigma(D^*\bar{D}^*)$ two contributions $D^{*0}\bar{D}^{*0} + D^{*+}\bar{D}^{*-}$, the $\sigma(D_s\bar{D}_s^*)$ two contributions, as the sum of $D_s^+\bar{D}_s^{*-} + D_s^{*+}\bar{D}_s^-$ meson–meson states. The $\sigma(D_s^+\bar{D}_s^-)$ includes only the $D_s^+\bar{D}_s^-$ meson–meson state. As we see in Fig. 7, the results for different sets of parameters do not change much. Now let us look in detail at the figure. The biggest contributions come from the $\sigma(D\bar{D}^*)$ and the $\sigma(D\bar{D})$ for the $\psi(4040)$. Conversely, the $\sigma(D^*\bar{D}^*)$ gives the biggest contribution in the region of the $\psi(4160)$, while the contribution from the other channels is small in the whole region. We have not considered the $D_s^*\bar{D}_s^*$ production which only contributes a small quantity at the very end of the $\psi(4160)$ resonance tail.

We refrain from a detailed comparison with experimental data which are somewhat conflicting in the different exper-

iments. Yet, it is instructive to look at the most recent measurements in Ref. [10]. By looking at Fig. 16 of Ref. [10] we can see that the D^+D^{*-} channel peaks around 4040 MeV as in our Fig. 7 and has a shoulder around 4160 MeV, as we also find in Fig. 7. These features are also observed in Fig. 4 of Ref. [4]. On the other hand, the $D^{*+}D^{*-}$ channel in Fig. 16 of Ref. [10] peaks around 4150–4200 MeV, as is also the case of our contribution of that channel in Fig. 7. The strength at the peaks of these two contributions filtering just the D^+D^{*-} and $D^{*+}D^{*-}$ channels in Fig. 7 is $\sim \frac{1}{4}5.5/\frac{1}{2}3 = 0.92$ versus $\sim 4/3 = 1.33$ in Ref. [10]. The agreement is fair.

With the caveat on the problem of conflict in the experiment, we nevertheless compare in Table 3 our results with the experimental ones of Ref. [11] and the theoretical ones, also using a $^3P_0$ model, of Ref. [2]. Note that the comparison is not all fair since we obtain the results of Fig. 7 from the interference of the two resonances. Our results in Table 3 refer to values of Fig. 7 at the peak of the $\psi(4040)$ and $\psi(4160)$ including the interference. The individual contributions in the theory of Ref. [2] come from single particle states and in the experiment from an analysis of data in Ref. [10], which are also in conflict with those of Ref. [9]. Hence, caution should be taken in the comparison to data in Table 3.

In addition to the caveat about comparing magnitudes which are not exactly the same, as discussed above, we should make some extra comments. The first one is that the theoretical errors quoted in Table 3 are only statistical. There should be systematic errors tied to the assumptions done, but these are more difficult to quantize. Our assumptions relying on the $^3P_0$ model to hadronize the $c\bar{c}$ state are rather standard and we do not rely upon a theoretical quark model but take input from experiment. Yet, there seems to be worse agreement in the case of the $\psi(4160)$ and part of it could be blamed on an approximation made in this case. Indeed, as shown in Eq. (A.8) of Ref. [15], for the case of d-wave resonances there is the possibility to have internal angular momentum $l = 1$ and $l = 3$. The $l = 3$ case involves quark matrix elements of $j_3(\hat{q})$ versus $j_1(\hat{q})$ for $l = 1$, and also goes with $Y_{3\mu}(\hat{q})$ instead of $Y_{1\mu}(\hat{q})$ implicit in Eq. (19). Making general assumptions of dominance of the lowest possible orbital angular momentum, the $l = 3$ component is neglected in [15] and here for the d-wave state. For the s-wave state only $l = 1$ is possible and that approximation is not done. In this latter case the weights $g_{R,i}^2$ of Table 1 coincide with those of Refs. [19–21]. In any case, we think that a better comparison with data, given the interference of the two resonances, should be done with the distributions for the different $D^{(*)}\bar{D}^{(*)}, D_s^{(*)}\bar{D}_s^{(*)}$, channels as a function of the energy, in the line discussed above comparing with data of Refs. [4,10]. New and more precise data improving on present ones and solving actual discrepancies would help to clarify the issue.

Table 3 Ratios of branching fractions for the $\psi(4040)$ and $\psi(4160)$ resonances

	Ref. [4]	Ref. [2]	Our results
1. $\mathcal{B}(\psi(4040) \to D\bar{D})/\mathcal{B}(\psi(4040) \to D^*\bar{D})$	$0.24 \pm 0.05 \pm 0.12$	0.003	0.54 ± 0.04
2. $\mathcal{B}(\psi(4040) \to D^*\bar{D}^*)/\mathcal{B}(\psi(4040) \to D^*\bar{D})$	$0.18 \pm 0.14 \pm 0.03$	1.0	0.18 ± 0.02
3. $\mathcal{B}(\psi(4160) \to D\bar{D})/\mathcal{B}(\psi(4160) \to D^*\bar{D}^*)$	$0.02 \pm 0.03 \pm 0.02$	0.46	0.56 ± 0.06
4. $\mathcal{B}(\psi(4160) \to D^*\bar{D})/\mathcal{B}(\psi(4160) \to D^*\bar{D}^*)$	$0.34 \pm 0.14 \pm 0.05$	0.011	0.60 ± 0.07

There are discrepancies of our results with the experimental analysis, particularly in the $D\bar{D}/D^*\bar{D}^*$ ratio of the $\psi(4160)$ where both the results of [2] and the present ones strongly disagree with the experimental analysis. In the other cases the present results are closer to the analysis than those of Ref. [2].

The formalism used in the present work is similar to the one used in [17] in the study of the $\psi(4040)$ resonance, earlier used also in the study of the lineshape of the $\psi(3770)$ [18], renormalizing the vector propagators by the meson–meson selfenergy. Apart from some technical details, the major difference is that the couplings of the resonance to the $D^{(*)}\bar{D}^{(*)}$ channels are taken from experiment (actually from the ratios of Table 3), while we have determined them theoretically by means of the $^3P_0$ model. A second major difference is that we have studied the $\psi(4040)$ in connection with the $\psi(4160)$ due to the strong interference between the two, while only the $\psi(4040)$ is considered in [17], although it is mentioned that for the purpose of their work, the investigation of a possible associated resonance, the consideration of the $\psi(4160)$ does not change much the results.

We can also do the compositeness test. In order to calculate the strength of the original vector when it is dressed by the meson–meson components we use the following formula (See detailed analysis in Ref. [15])

$$Z = \frac{1}{1 - \frac{\partial Re \Pi(p^2)}{\partial p^2}\Big|_{p^2 = M_R^2}}. \tag{26}$$

On the other hand $1 - Z$ provides the meson–meson strength of the dressed vector.[1] If $\frac{\partial Re \Pi(p^2)}{\partial p^2}$ is quite smaller than 1, we can make the following expansion

$$1 - Z \simeq -\frac{\partial Re \Pi}{\partial p^2}\Big|_{p^2 = M_R^2}, \tag{27}$$

where $-\frac{\partial Re \Pi}{\partial p^2}\Big|_{p^2 = M_R^2}$ reads as the meson–meson strength

in the wave function and it can be written for each channel as

$$P_{(MM)i} \simeq -\frac{\partial Re \Pi_i(p^2)}{\partial p^2}\Big|_{p^2 = M_R^2}, \tag{28}$$

where Π_i is the contribution of the i-th channel to Π. We calculate the meson–meson weight and show the results using the results of Set I in Tables 4 and 5 for the $\psi(4040)$ and $\psi(4160)$, respectively. The value of Z shown there is obtained from Eq. (26) and includes the contributions from all channels.

As we can see in Tables 4 and 5, we obtain some negative results for the $P_{(MM)}$, which should not come as a big surprise since the weights have not to be identified with a probability, as discussed in detail in [15]. For the closed channels, where the identification of weight with probability is fair, we obtain positive numbers. The interesting result, however, is that all these numbers are very small, which make these vector mesons to qualify as mostly $c\bar{c}$ states with a very small meson–meson cloud component.

4 Summary and conclusions

We have made a fit to the $e^+e^- \to hadron$ data in the region of the $\psi(4040)$ and $\psi(4160)$ resonances, considering the hadronic channels $D\bar{D}$, $D\bar{D}^*$, $D^*\bar{D}$, $D^*\bar{D}^*$, $D_s\bar{D}_s$, $D_s\bar{D}_s^*$, $D_s^*\bar{D}_s$, $D_s^*\bar{D}_s^*$. We have taken into account the renormalization of the vector mesons by including the meson–meson selfenergy, and the scheme provides automatically the cross sections into the different channels. We had some freedom fitting the data by means of a few parameters, but the relative weight of the different channels was calculated theoretically by means of the $^3P_0$ model, hence the relative ratios for production of the different channels is a prediction of the theory. The sometimes conflicting experimental results do not allow a quantitative comparison with experiment, but the agreement with the most recent experimental data is fair. We have also explored a side effect of the theory by evaluating the weights of the different meson–meson components in the wave function and determined that the $\psi(4040)$ and $\psi(4160)$ have very small meson–meson components and largely qualify as $c\bar{c}$ states. Improved rates of

---

[1] In Ref. [15] a thorough discussion is made of the meaning of the strengths of the meson–meson channel, which measures the weight of each channel in the wave function, but cannot be associated to a probability, except if the channel is closed.

Table 4 Meson–meson probabilities in the $\psi(4040)$ wave function for Set I

Channels	$-\frac{\partial \Pi}{\partial p^2}\big|_{p^2=M^2_{\psi(4040)}}$	$P_{(MM)}$	Z
$D^0\bar{D}^0$	$(-1.499 + 1.065i) \times 10^{-2}$	-1.499×10^{-2}	
D^+D^-	$(-1.434 + 1.054i) \times 10^{-2}$	-1.434×10^{-2}	
$D^0\bar{D}^{*0} + c.c$	$(-2.816 + 3.499i) \times 10^{-2}$	-2.816×10^{-2}	
$D^+\bar{D}^{*-} + c.c$	$(-2.654 + 3.437i) \times 10^{-2}$	-2.654×10^{-2}	
$D^{*0}\bar{D}^{*0}$	$(-1.572 \times 10^{-3} + 3.267i \times 10^{-2})$	-1.572×10^{-3}	
$D^{*+}D^{*-}$	$(2.108 \times 10^{-3} + 2.968i \times 10^{-2})$	2.108×10^{-3}	
$D_s^+D_s^-$	$(-4.026 + 7.377i) \times 10^{-3}$	-4.026×10^{-3}	
$D_s^+D_s^{*-} + c.c$	$(1.591 \times 10^{-3} + 2.366i \times 10^{-5})$	1.591×10^{-3}	
$D_s^{*+}D_s^{*-}$	$(8.467 \times 10^{-4} + 4.427i \times 10^{-6})$	8.467×10^{-4}	
Total	$(-0.0851 - 0.0160i)$	-0.0851	0.91

Table 5 Meson–meson probabilities in the $\psi(4160)$ wave function for Set I

Channels	$-\frac{\partial \Pi}{\partial p^2}\big|_{p^2=M^2_{\psi(4160)}}$	$P_{(MM)}$	Z
$D^0\bar{D}^0$	$(-1.155 \times 10^{-2} + 5.296i \times 10^{-3})$	-1.155×10^{-2}	
D^+D^-	$(-1.107 \times 10^{-2} + 5.339i \times 10^{-2})$	-1.107×10^{-2}	
$D^0\bar{D}^{*0} + c.c$	$(-6.171 + 5.157i) \times 10^{-2}$	-6.171×10^{-2}	
$D^+\bar{D}^{*-} + c.c$	$(-5.934 + 5.141i) \times 10^{-3}$	-5.934×10^{-3}	
$D^{*0}\bar{D}^{*0}$	$(-2.057 + 3.648i) \times 10^{-2}$	-2.057×10^{-2}	
$D^{*+}D^{*-}$	$(-1.939 + 3.624i) \times 10^{-2}$	-1.939×10^{-2}	
$D_s^+D_s^-$	$(-4.471 + 5.007i) \times 10^{-3}$	-4.471×10^{-3}	
$D_s^+D_s^{*-} + c.c$	$(-1.127 + 4.361i) \times 10^{-3}$	-1.127×10^{-3}	
$D_s^{*+}D_s^{*-}$	$(8.845 \times 10^{-3} + 1.423i \times 10^{-4})$	8.845×10^{-3}	
Total	$(-7.145 \times 10^{-2} + 0.103i)$	-7.145×10^{-2}	0.93

production of these channels in the future should allow for a more quantitative comparison, and agreement or disagreement with data can shed light on possible mixing of the $c\bar{c}$ charmonium states with other configurations, a topic of current interest.

Data Availability Statement This manuscript has no associated data or the data will not be deposited. [Authors' comment: All data generated during this study are contained in this published article.]

References

1. E. Eichten, K. Gottfried, T. Kinoshita, K.D. Lane, T.M. Yan, Phys. Rev. D **21**, 203 (1980)
2. T. Barnes, S. Godfrey, E.S. Swanson, Phys. Rev. D **72**, 054026 (2005)
3. M. Ablikim et al., [BES Collaboration]. eConf C **070805**, 02 (2007). [Phys. Lett. B **660**, 315 (2008)]
4. B. Aubert et al., BaBar Collaboration. Phys. Rev. D **79**, 092001 (2009)
5. S. Godfrey, N. Isgur, Phys. Rev. D **32**, 189 (1985)
6. J. Segovia, D.R. Entem, F. Fernandez, E. Hernandez, Int. J. Mod. Phys. E **22**, 1330026 (2013)
7. P.G. Ortega, J. Segovia, D.R. Entem, F. Fernández, Phys. Lett. B **778**, 1 (2018)
8. G. Goldhaber et al., Phys. Lett. **69B**, 503 (1977)

9. D. Cronin-Hennessy et al., CLEO Collaboration. Phys. Rev. D **80**, 072001 (2009)

10. V. Zhukova et al., [Belle Collaboration]. Phys. Rev. D **97**(1), 012002 (2018)

11. J.Z. Bai et al., BES Collaboration. Phys. Rev. Lett. **84**, 594 (2000)

12. J.Z. Bai et al., BES Collaboration. Phys. Rev. Lett. **88**, 101802 (2002)

13. X.H. Mo, C.Z. Yuan, P. Wang, Phys. Rev. D **82**, 077501 (2010)

14. A. Bramon, A. Grau, G. Pancheri, Phys. Lett. B **283**, 416 (1992)

15. Q.X. Yu, W.H. Liang, M. Bayar, E. Oset, Phys. Rev. D **99**(7), 076002 (2019)

16. J.M. Blatt, V.F. Weisskopf, *Theoretical nuclear physics* (Springer, New York, 1979)

17. M. Piotrowska, F. Giacosa, P. Kovacs, Eur. Phys. J. C **79**, 98 (2019)

18. S. Coito, F. Giacosa, Nucl. Phys. A **981**, 38 (2019)

19. A. De Rujula, H. Georgi, S.L. Glashow, Phys. Rev. Lett. **37**, 398 (1976)

20. E. van Beveren, G. Rupp,. arXiv:0910.0967 [hep-ph]

21. E. van Beveren, C. Dullemond, G. Rupp, Phys. Rev. D **21**, 772 (1980). Erratum: [Phys. Rev. D **22**, 787 (1980)]